Electrochimica Acta 490 (2024) 144269

Contents lists available at ScienceDirect

Electrochimica Acta

journal homepage: www.journals.elsevier.com/electrochimica-acta

Effect of the synthesis route and Co Coverage on Co / $Ti_3C_2T_x$ materials for the oxygen evolution reaction

Can Kaplan [a], Ricardo Mogollon Restrepo [a], Thorsten Schultz [b,c], Ke Li [d], Valeria Nicolosi [d], Norbert Koch [b,c], Michelle P. Browne [a,*]

[a] Helmholtz Young Investigator Group Electrocatalysis: Synthesis to Devices, Helmholtz-Zentrum Berlin für Materialmen und Energie, 14109 Berlin, Germany
[b] Helmholtz-Zentrum Berlin für Materialien und Energie GmbH, Berlin, 14109, Germany
[c] Institut für Physik & IRIS Adlershof, Humboldt-Universität zu Berlin, Berlin, Germany
[d] School of Chemistry, CRANN and AMBER Research Centres, Trinity College Dublin, College Green, Dublin D02 PN40, Ireland

ARTICLE INFO

Keywords:
Alkaline water splitting
Oxygen evolution reaction (oer)
MXenes
Co Hydroxide
Co-LDH

ABSTRACT

Green hydrogen resulting from water electrolysis is a key component for the transition to a renewable energy economy. However, it's success highly depends on active and stable electrocatalysts for the oxygen evolution reaction (OER) which is the bottleneck reaction of water electrolysis. Herein we assess the OER performance of non-noble metal-based electrocatalysts comprising Co oxide/hydroxide and delaminated 2D transition metal carbide sheets, $Ti_3C_2T_x$ MXene. The catalytically active sites are provided by Co oxide/hydroxide, while the MXene contributes exceptional electrical conductivity. Our comprehensive electrochemical evaluation of their OER performance reveals that the chemical functionalization of Co on MXene sheets outperforms the pure Co or MXene alone, as well as physically mixed materials, across all tested performance metrics. From the materials characterisation, the chemical functionalized Co/$Ti_3C_2T_x$ materials exhibit increased formation of layered double hydroxide (LDH) $Co(OH)_2$ structures compared to the pure Co and physically mixed materials which may result in the improved OER activity observed for these materials. These findings emphasize the potential of anchoring transition metal oxides/hydroxides on MXene as a superior OER electrocatalyst for advancing sustainable green hydrogen production.

1. Introduction

Water splitting, the process of dividing water into its constituent elements, hydrogen and oxygen, through electrolysis, is a process at the forefront of green energy initiatives, particularly in the context of producing clean and renewable hydrogen for various applications [1]. One crucial aspect of water splitting lies in the oxygen evolution reaction (OER), where the development of efficient electrocatalysts is imperative for enhancing the overall performance of water electrolysis systems [2]. This is because the OER exhibits sluggish kinetics which makes this reaction the bottleneck of water electrolysis. Finding low-cost, stable, and efficient OER catalysts is vital for reducing energy losses and improving the economic feasibility of green hydrogen production. Hence, there is a pressing need to explore and develop advanced materials that can catalyse the OER with high activity, stability, and cost-effectiveness.

Selecting the appropriate metal oxides for OER electrocatalysis involves a delicate balance of factors such as conductivity, stability, and catalytic activity. Transition metal oxides (TMOs) have garnered substantial attention due to their promising electrocatalytic properties [3]. To date, the most effective OER catalysts reported for acidic media are oxides based on iridium and ruthenium, both of which are precious metals [4]. In contrast, in alkaline conditions, cheaper and more abundant 3d transition metals can serve as catalysts as their oxides and hydroxides remain thermodynamically stable [2]. Consequently, various materials incorporating iron, nickel, manganese, or cobalt have shown good catalytic performance for the OER [2].

Out of the numerous crystallographic phases these 3d transition metals can exist in, the layered double hydroxide (LDH) family of materials has emerged as promising candidates. LDHs based on cobalt, chromium, nickel, iron, manganese, or their alloys have already been reported as efficient catalysts for the OER in alkaline media [5–7]. The general formula for LDH can be represented as $[M^{2+}_{1-x}M^{3+}_{x}(OH)_2]^{x+}[A_{x/n}]^{n-}\cdot mH_2O$ where M^{2+} and M^{3+} denote divalent

* Corresponding author.
E-mail address: Michelle.browne@helmholtz-berlin.de (M.P. Browne).

https://doi.org/10.1016/j.electacta.2024.144269
Received 17 January 2024; Received in revised form 28 March 2024; Accepted 13 April 2024
Available online 17 April 2024
0013-4686/© 2024 The Authors. Published by Elsevier Ltd. This is an open access article under the CC BY license (http://creativecommons.org/licenses/by/4.0/).

and trivalent metal cations, respectively [8]. The hydroxide ions coordinate with these metal cations to form positively charged brucite-like layers. The interlayer space accommodates intercalated anions A^{n-} which compensate the positive charge of the main layer. This layered structure enables facile ion exchange and provides active sites for catalytic reactions [3].

However, while LDH materials exhibit promising catalytic activity for certain reactions, these materials generally suffer from a poor intrinsic electronic conductivity [9]. Being composed of metal cations and hydroxide anions, the electronic conductivity of LDH materials relies largely on charge transfer processes between different metal cations in the layered structure [10]. This limits their performance as electrocatalysts in reactions with stringent conductivity requirements such as the OER. One strategy to enhance the electronic conductivity of LDHs comprises the introduction of conductive additives (e.g. carbon nanotubes (CNT)) [11] creating composite materials. This approach addresses the weakness of limited intrinsic electronic conductivity thereby improving the overall electrocatalytic performance of LDHs. However, carbon based additives can corrode under potentials relevant for OER and the associated anodic current can confound the interpretation of OER activity [12].

In this regard, MXenes with their unique combination of high electronic conductivity (8000–10 000 S cm^{-1}) [13,14], hydrophilicity, and tuneable surface chemistry have attracted much attention as promising supports for enhancing the performance of metal oxides in catalysing the OER [15–17]. MXenes are a family of two-dimensional (2D) transition metal carbides, nitrides, or carbonitrides, first discovered in 2011 [18]. Their hexagonal structure consists of a succession of M_6X octahedra layers with the general formula $M_{n+1}X_nT_x$, where M is a transition metal (e.g., Ti, V, Nb), X is carbon and/or nitrogen and n is the number of layers. T_x is usually added to represent the surface terminations resulting from the synthesis process, such as -OH, -O, or -F termination groups [18]. MXenes are typically derived from MAX phases, layered ternary carbides or nitrides of the general formula $M_{n+1}AX_n$, in a process involving selective etching of the 'A' layer (group III-A or IV-A elements) from the MAX phase, leaving behind the 2D MXene structure. The surface terminations T_x are formed during this exfoliation step and are controlled by the exfoliation conditions [13,19,20]. These surface terminations are potential anchoring points for catalytically active particles/materials. In particular, -OH and -O groups can form strong chemical bonds with metal oxides, enhancing dispersion of metal nanoparticles on the MXene surface, preventing agglomeration, and promoting a uniform distribution of catalytic sites. Furthermore, these chemical bonds enable charge transfer between the MXene and the metal oxide nanoparticles, improving the overall conductivity and catalytic activity of the composite [21].

Among the numerous possible elemental combinations arising from the formula $M_{n+1}X_nT_x$, titanium carbide ($Ti_3C_2T_x$) was the first successfully synthesized MXene and as such, naturally a focal point of research. In several works it has been showcased as a promising support for metal oxide-based catalysts for OER such as Co_3O_4 [22], FeNi-LDH [23], CoFe-LDH [24], $MnCo_2O_4$ [25], $CuCoO_4$ [26], and $Co(OH)_2$ [27]. Prior investigations into Co hydroxide/MXene composites have shown promise, with reported improvements in OER catalytic activity attributed to the synergistic effects between the Co species and the unique properties of MXenes [15]. In literature, Co hydroxide/MXene composites have been synthesized by various methods including chemical functionalization and physical mixing. Benchakar et al. show that by chemically functionalizing Co hydroxide structures onto $Ti_3C_2T_x$, the resulting materials achieve an overpotential of 330 mV at a current density of 10 mA cm^{-2}, which out-performed the bare Co hydroxide, the bare $Ti_3C_2T_x$ and the state-of-the-art IrO_2 catalyst [15]. Furthermore, Tyndall et al. report an improvement of the overpotential by 180 mV at 10 mA cm^{-2} after physically mixing a Co hydroxide catalyst with 1 % $Ti_3C_2T_x$MXene [27]. However, a comprehensive understanding of the optimization strategies for maximizing OER performance in Co/MXene composites is still evolving. In this work, we delve into the synthesis of MXene supported Co hydroxide nanocrystals by comparing chemically functionalized and physically mixed Co hydroxide/MXenes at various MXene concentrations to understand how important the synthesis method and concentration of MXene is on the OER for the same Co oxide/hydroxide material.

Herein, we present a comprehensive electrochemical investigation of $Co/Ti_3C_2T_x$ based electrocatalysts. We address key gaps in understanding how the Co content and fabrication route can affect the OER and characterize them under extensive electrochemical methods, eliciting important and previously unexplored performance metrics, e.g., turnover frequency, stability, faradaic efficiency, and electrochemical surface area. The insights derived from our electrochemical analyses not only contribute to the growing fundamental knowledge of $Co/Ti_3C_2T_x$ based electrocatalysts but also hold potential implications for optimizing the design of MXene supported TMO materials for efficient and sustainable water electrolysis.'

2. Experimental

2.1. Synthesis of materials

Synthesis of $Ti_3C_2T_x$: Ti_3AlC_2 MAX phase (1 g, 5.1 mmol, 400 mesh, Carbon, Ukraine) was added over 10 min into a solution mixture consisting of LiF (1 g, 38.5 mmol, Sigma-Aldrich) and 9 M HCl (20 mL, Sigma-Aldrich) and stirred at 35 °C for 48 h, yielding multilayer $Ti_3C_2T_x$. The mixture was then washed with deionized water by repeatedly centrifuging at 3005 × *g* and discarding the supernatant until pH neutrality. To produce few-layer $Ti_3C_2T_x$, the as-synthesized multilayer $Ti_3C_2T_x$ was redispersed in deionized water and sonicated for 1 h in an ice bath with N_2 bubbling. After another centrifugation at 3005 × *g* for 1 h, black coloured few-layer $Ti_3C_2T_x$ dispersion was collected which was freeze dried to obtain a few-layer $Ti_3C_2T_x$ foam.

Synthesis of pure Co, CF0.39, CF0.56 and preparation of PM0.39 and PM0.56: The Co/ $Ti_3C_2T_x$ ratio was chosen to obtain a high coverage of the MXene in the final product. Assuming the final composition of the Co/MXene composite material as $Co(OH)_2$ and $Ti_3C_2(OH)_2$, the amount of MXene was selected to obtain the final Co/Ti atomic ratios of 1.2 and 0.6 corresponding to 3.6 and 1.8 Co atoms per $Ti_3C_2(OH)_2$ unit and $Ti_3C_2(OH)_2$wt ratios of 39 wt.% and 56 wt.%. To synthesize the chemically functionalized composites **CF0.39** and **CF0.56**, $Ti_3C_2T_x$ foam (38 mg, 76 mg respectively) was first dispersed in ethylene glycol (35 mL, 99.8 %, Sigma Aldrich) under stirring in N_2 atmosphere for 10 min. Then, anhydrous Co (II) acetate (114 mg, 0,644 mmol, 99.99 %, Sigma-Aldrich) was added to this suspension. After 30 min, NaOH (26 mg, 0.65 mmol, ≥97 %, Sigma-Aldrich) was added and the mixture was stirred under N_2 overnight at room temperature. The solution was then transferred into a sealed autoclave and heated at 200 °C for 3 h. The product was first centrifuged at 3069 × *g* for 15 min and then repeatedly washed and centrifuged with ethanol (1 ×) and deionized water (3 ×) discarding the supernatant after each centrifugation. The sediment was dried overnight at 60 °C. The pure Co sample was produced in the same way, but without the addition of MXene. **PM0.39** and **PM0.56** were prepared by physically mixing appropriate ratios of pure Co and $Ti_3C_2T_x$ containing dispersions.

2.2. Materials characterisation

X-ray diffractograms were recorded using a Bruker D8 ADVANCE powder diffractometer using Cu $K_{\alpha1}$ ($\lambda = 0.1541$ nm), and $K_{\alpha2}$ radiation source ($\lambda = 0.1544$ nm). Diffraction patterns were collected between 5° and 100° applying a step size of 0.0131° and a step time of 1.5 s. Scanning electron micrographs were obtained on a Zeiss MERLIN 0.1–30 keV field emission gun scanning electron microscopes. Samples were prepared by drop casting an ink dispersion containing 0.16 mg of the relevant material onto an aluminium specimen holder and drying it

under a stream of nitrogen. X-Ray Photoelectron Spectroscopy (XPS) measurements were conducted using a JEOL JPS-9030 setup with a base pressure of $2\bullet10^{-9}$ mbar. Samples were prepared by spray coating an Au/Ti coated Si/SiO_2 wafer with an ink dispersion made up of 10 mg of the relevant catalyst material in 496 μl of H_2O, 496 μl of iPrOH and 8 μl of Nafion solution. A non-monochromated Al source with 300 W power was used for excitation and a hemispherical analyser with pass energy of 50 eV (surveys) and 20 eV (narrow scans) was used to detect the emitted photoelectrons. The analyser binding energy scale was calibrated by measuring sputter cleaned gold and copper foils just before the measurements and setting the $Au4f_{7/2}$ peak to 84.00 eV and the $Cu2p_{3/2}$ peak to 932.62 eV. Since the samples exhibited charging, the C1s C-Ti component of the samples containing Ti_3C_2 was set to 282.0 eV for comparison. This yielded a binding energy of the C-F component of the Nafion of 291.7 eV, which was used to calibrate the binding energy of the samples not containing Ti_3C_2. For post OER spectra, 1 cm^2 of the wafer was immersed into a 1 M NaOH electrolyte solution and was held at a constant current of 10 mA cm^{-2} for 1 h prior to XPS measurements.

2.3. Electrochemical characterisation

Electrochemical experiments were typically conducted using a CHI760E potentiostat and a standard three-electrode cell consisting of a glassy carbon (GC) rotating disc electrode (RDE) with the catalyst as the working electrode, a Hg/HgO reference electrode and a carbon rod as the counter electrode. The electrodes were immersed into a nitrogen-saturated 1 M NaOH electrolyte solution.

For RDE experiments, GC RDEs with an electrode area of 0.0707 cm^2 were used. 2.26 μl of an ink dispersion made up of 10 mg of the relevant catalyst material in 496 μl of H_2O, 496 μl of iPrOH and 8 μl of Nafion solution was drop cast onto the GC electrode and dried at room temperature, resulting in a catalyst loading of 0.32 mg cm^{-2}. The electrodes were immersed into a 1 M NaOH electrolyte solution. Routinely before other measurements, cyclic voltammetry (CV) was performed at a scan range of −0.4 – 0.6 V, and a scan rate of 40 mV s^{-1}. Linear sweep voltammetry (LSV) measurements were conducted at a scan range of 0 − 0.8 V vs. Hg/HgO and a scan rate of 1 mV s^{-1}. All measurements were IR-drop corrected by determining the cell resistance via electrochemical impedance spectroscopy (EIS) measured at a potential of 0 V vs. Hg/HgO (non-Faradaic region) from 1 MHz to 1 Hz. For measuring the charge transfer resistance (R_{ct}), EIS was conducted at a potential of 0.8 V vs. Hg/HgO. Double layer capacitance was measured by running multiple CVs over a scan range of 100 mV with the scan rate ranging from 1 to 100 mV s^{-1}. The respective currents measured in a flat region (non-Faradaic) of the scan range were then plotted against the scan rate and the double layer capacitance was determined from the slope of this plot. Chronopotentiometry was conducted at a constant current of 10 mA cm^{-2} until material degradation.

Faradaic efficiency (FE) was measured using a rotating ring-disc electrode (RRDE) with a GC disk with an area of 0.1257 cm^2 and a platinum ring with an area of 0.1885 cm^2. Linear sweep voltammetry was conducted on the disk at a scan range of 0 − 0.8 V vs. Hg/HgO and a scan rate of 1 mV s^{-1} while the ring was held at a constant reducing potential of −0.63 V vs Hg/HgO. The collection efficiency of the ring electrode was experimentally determined prior to the measurement [28]. The potentials measured vs. Hg/HgO were mathematically converted to overpotential η using the equation $E = E_{Hg/HgO} + 0.059\ pH + E^0_{Hg/HgO} + E^0$, where $E_{Hg/HgO}$ is the standard Hg/HgO electrode potential equal to 0.098 V at 25 °C and E^0 is the standard cell potential of OER and is equal to 1.23 V.

3. Results and discussion

3.1. Synthesis and characterisation of materials

In this study, Co/MXene materials were prepared by two different fabrication routes (chemical functionalization and physical mixing), Scheme 1, and two MXene loadings (39 wt% and 56 wt%, excluding the pure MXene (100 wt%) material) in order to study how these parameters can affect OER performance. For both routes, first, the $Ti_3C_2T_x$ (MXene) was produced by etching the Ti_3AlC_2 by in-situ exfoliation with LiF and HCl to produce multi-layer $Ti_3C_2T_x$ and then exfoliated to achieve few-layer $Ti_3C_2T_x$ [29].

For the first route, chemical functionalization, the MXene composites materials are labelled as **CF0.39** (MXene loading of 39 wt%) and **CF0.56** (MXene loading of 56 wt%), Scheme 1, route 1. For this route, the $Ti_3C_2T_x$ MXene flakes added to the ethylene glycol solution of Co(II) precursor were first treated with sodium hydroxide and then subjected to a solvothermal treatment to grow a Co hydroxide phase (see Experimental Section, adapted from Benchakar et al.) [15]. For the second route, physical mixing (Scheme 1, route 2) the MXene composites, denoted as **PM0.39** and **PM0.56**, were prepared by physical mixing of Co hydroxide and $Ti_3C_2T_x$ containing dispersions.

Scanning electron microscope (SEM) micrographs of relevant materials are depicted in Fig. 1. Micrographs of the $Ti_3C_2T_x$ starting material (Fig. 1a) exhibit the typical 2D-like MXene morphology of tightly stacked sheets as reported for MXene synthesized with the etching method that involves the use of LiF/HCl [13,30]. Micrographs of the pure Co sample (Fig. 1b) show flower like agglomerates of roughly 2–4 μm diameter composed of Co oxide/hydroxide nanosheets.

In the chemically functionalized composites similar spherical morphologies were found which preferably agglomerated on the surface of the MXene sheets seemingly forming an interconnected porous network (Fig. 1c-d). Additional growth of Co oxide/hydroxide covering the MXene surface was further discernible. Even though surface coverage of the MXene was not quantified, during the SEM observation of sample **CF0.39** (Fig. 1c) it can be noted that most of the MXene surface appeared to be covered with Co hydroxide while in micrographs of sample **CF0.56** (Fig. 1d) many exposed MXene sheets were observed. This suggests that Co/Ti ratios lower than 1.2 lead to insufficient coverage of the MXene surface. Furthermore, in the physically mixed reference samples (Fig. 1e and f) the almost complete absence of Co oxide/hydroxide on the surface of the MXene was noted. These findings demonstrate the necessity and the success of the chemical anchoring of Co oxide/hydroxide onto the MXene surface via the solvothermal procedure used herein.

X-ray photoelectron spectroscopy results for all materials are shown in Fig. 2. From the Co2p region (Fig. 2a), all of the materials which used the Co salt precursor during the synthesis step, have now transformed into either CoO or $Co(OH)_2$. A distinction from the Co2p region alone is not possible (compare Biesinger et al.) [31]. While the Co2p spectra of the CF samples are virtually identical, the satellite peak at ~788 eV is slightly weaker for the PM samples, indicating a difference in the Co oxide structure for those two preparation routes. The Ti-C peaks at 282 eV (C1s) as well as the titanium peak at 455 eV (Ti2p) are clear indications of the formation of $Ti_3C_2T_x$ MXene and are also visible for both CF and PM samples.

The X-ray diffraction (XRD) patterns of the $Ti_3C_2T_x$, pure Co and the composite materials recorded with a Cu K_α radiation source are presented in Fig. 3. The diffraction peaks obtained for the $Ti_3C_2T_x$ sample (Fig. 3a) at positions 6.2, 17.82, 29.0, 35.62, 42.59 and 60.76 ° are in good agreement with reported patterns for $Ti_3C_2T_x$ MXene prepared via LiF/HCl etching [32,33]. Additionally, weak diffraction peaks at 2θ values of 10.68 and 21.5 ° show that only residual amounts of the initial Ti_3AlC_2 MAX phase remained in the sample; while most of the starting material was etched yielding the $Ti_3C_2T_x$ MXene.

The diffraction pattern of the pure Co sample (Fig. 3b) indicates a mixture of two phases. A primary phase of $Co(OH)_2$ with characteristic

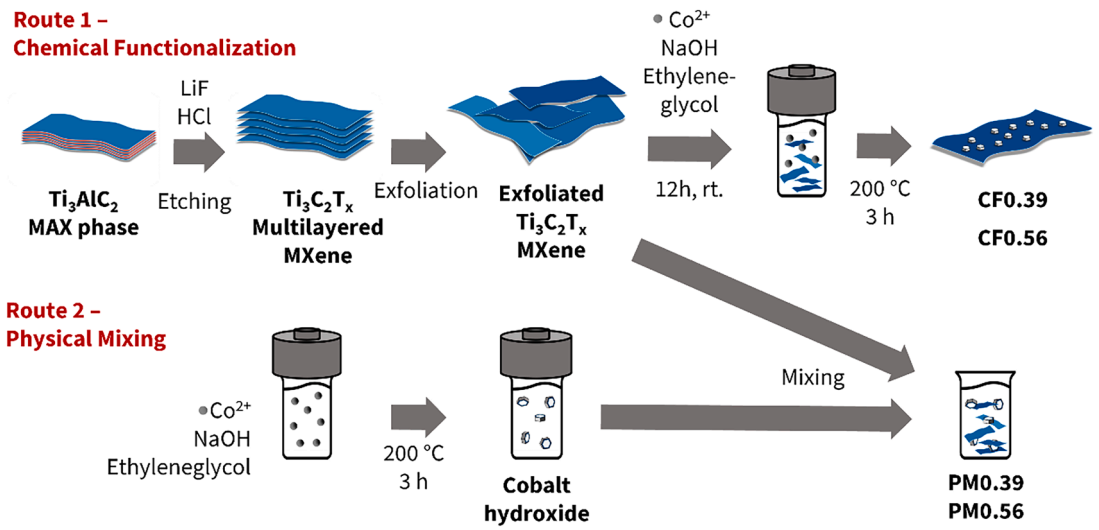

Scheme 1. Preparation routes to $Ti_3C_2T_x$ MXenes, MXene supported Co oxide/hydroxide and physically mixed reference materials.

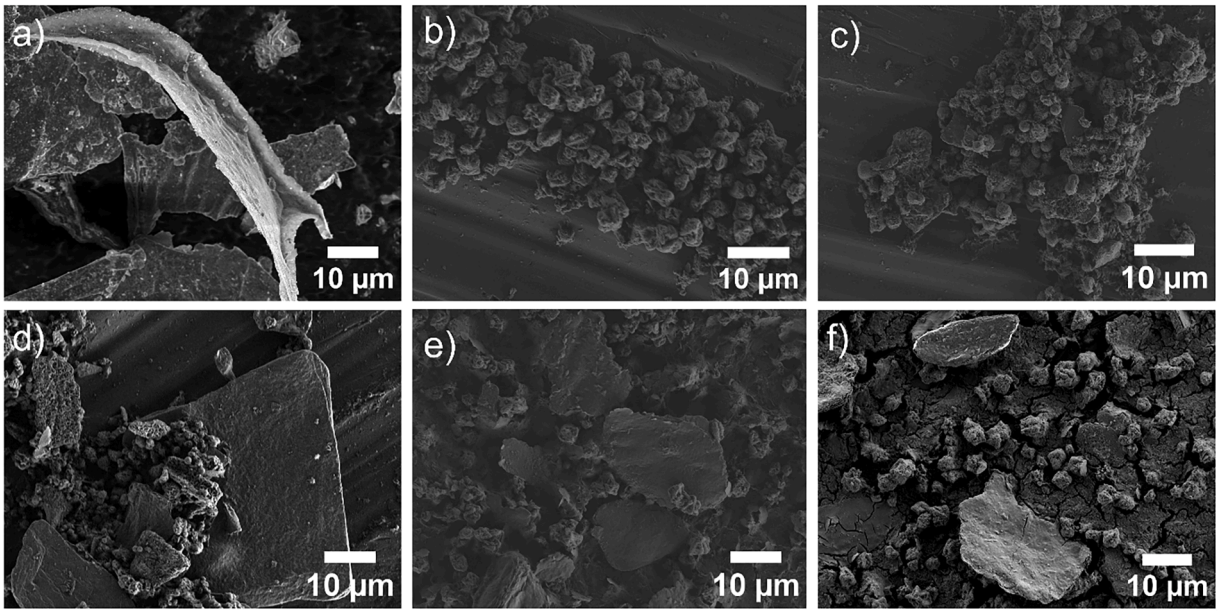

Fig. 1. Scanning electron micrographs of a) $Ti_3C_2T_x$, b) pure Co, c) **CF0.39**, d) **CF0.56**, e) **PM0.39** and f) **PM0.56**.

peaks at 18.81, 32.52, 37.88, 51.24, 58.1, 61.6, 69.08 and 71.59° (JCPDS no. 30–0444) and a secondary hydrotalcite like phase of Co-LDH with peaks at 10.41, 34.5, 44.43 ° and a shoulder at 20.91 °, (JCPDS no. 53–0917). In the diffraction patterns of the chemically functionalized composites (Fig. 3c), the intense (002) peak at 6.2° as well as the absence of a diffraction line at 25.23° typical for TiO_2 confirm the preservation of the oxidation sensitive MXene during the solvothermal process [34]. In contrast to the patterns of the pure Co and the physically mixed materials (Fig. 3d), in the $Ti_3C_2T_x$ supported materials the intense peaks characteristic for $Co(OH)_2$ (JCPDS no. 30–0443) at 18.8, 32.5 and 38.0 ° were weaker or not found. This suggests that the MXene instead promotes the formation of Co-LDH also evidenced by the peak at 10.63° characteristic for the hydrotalcite like phase for the materials made by chemical functionalization and is further promoted by a lower wt% of MXene.

3.2. Electrochemical evaluation

The electrochemical behaviour of the pure Co, $Ti_3C_2T_x$ and the Co/MXene composite materials were characterized in a nitrogen-saturated 1 M NaOH electrolyte.

First, cyclic voltammetry (CV) was conducted at a scan rate of 40 mV s^{-1} as presented in Fig. 4. In the pure $Ti_3C_2T_x$ sample, an irreversible oxidation peak was observed at around 0.91 V versus the reference hydrogen electrode (RHE). This peak can be attributed to the Ti(III)/Ti (IV) redox transition [35]. For the pure Co sample, an irreversible oxidation peak at 1.50 V vs. reference hydrogen electrode (RHE) was observed, indicating Co(II)/Co(III) and Co(III)/Co(IV) redox transitions that cause the formation of active sites for OER [36,37]. This Co oxidation peak is still discernible in the composite materials **CF0.39** and **CF0.56** where it was shifted by 0.1 V to a lower potential and its intensity decreases with the Co content. For the physically mixed composites **PM0.39** and **PM0.56** the Co peak appeared much weaker and gradually decreased in further CV cycles (Figure S1). It is unclear what

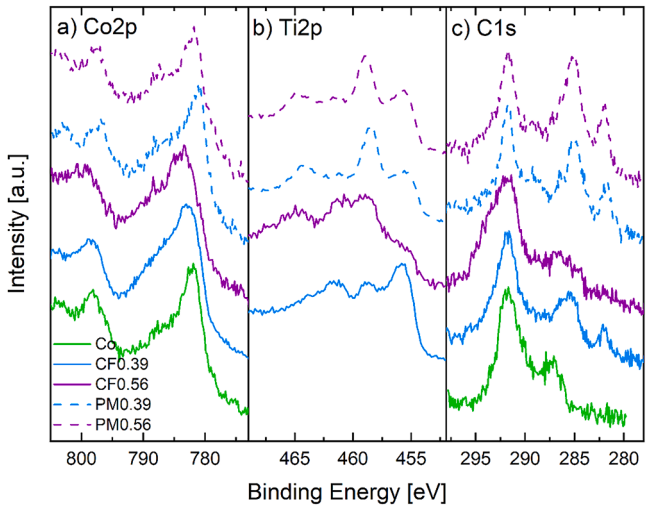

Fig. 2. X-ray Photoelectron spectra of pure Co and chemically functionalized (CF) and physically mixed (PM) composite materials. a) Co2p, b) Ti2p, and c) C1s core levels.

causes this decrease; however, a possible explanation could be the loss of conductivity of the catalysts layer caused by oxidation of the MXene or the MXene covering the Co oxide OER active material. However, after the first cycle the Co(I)/Co(II) transition at 1.05 V vs. RHE is observed which shows that the Co sites are exposed.

For the composite materials **CF0.39** and **CF0.56** no Ti(III)/Ti(IV) oxidation peak was registered at this potential, while for the physically mixed reference materials the Ti-oxidation peak was clearly visible. This seems to suggest that surface functionalization of the $Ti_3C_2T_x$ with Co oxide/hydroxide prevents the oxidation of the MXene, which is in agreement with previous characterisations. Therefore, anchoring the Co oxide/hydroxide phase by a chemical method is clearly necessary to establish a protective surface layer for the MXene, as physical mixing of the components seems insufficient to prevent MXene oxidation.

One of the key parameters used to evaluate the performance of an OER electrocatalyst is the overpotential required to achieve the benchmark current density of 10 mA cm^{-2}, η_{10} [38]. For this, linear sweep voltammograms (LSVs) using a rotating disk electrode set at a rotating rate of 1600 rpm at a scan rate of 1 mV s^{-1} were recorded. The obtained LSV curves and overpotentials (η_{10}) error bars are depicted in Fig. 5a and b, respectively. The much lower η_{10} values of **CF0.39** (387 mV) and **CF0.56** (398 mV) compared to unsupported Co (432 mV) indicate the increased electrocatalytic activity of the composite materials.

No such improvement was observed with the physically mixed composites, both showing higher overpotentials than the pure Co material. Normalizing the current by the geometric area can provide an inaccurate representation of the electrocatalytic activity, as not all of the electrode's geometric area is necessarily involved in the electrochemical reactions, i.e., parts of the electrode surface might be covered by insulating layers or not covered at all, thus not contributing to the catalytic reaction. Therefore, normalizing by the electrochemical surface area (ECSA) addresses this limitation by considering only the active surface area where the electrochemical reactions take place. ECSA was calculated by dividing the double layer capacitance of the catalyst layer C_{dl}, which was determined as described in the experimental section, by the material's specific capacitance C_F which for transition metals in 1 M

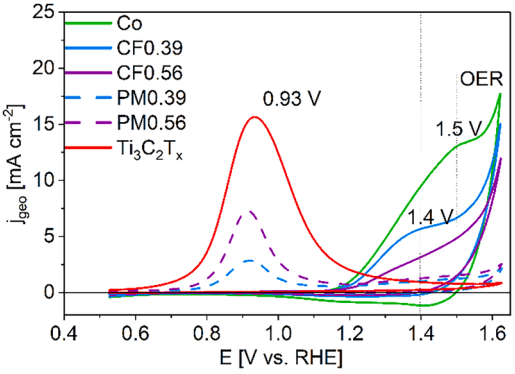

Fig. 4. Cyclic voltammograms of $Ti_3C_2T_x$, pure Co and physically mixed and chemically functionalized Co /$Ti_3C_2T_x$ composite materials. (first scans).

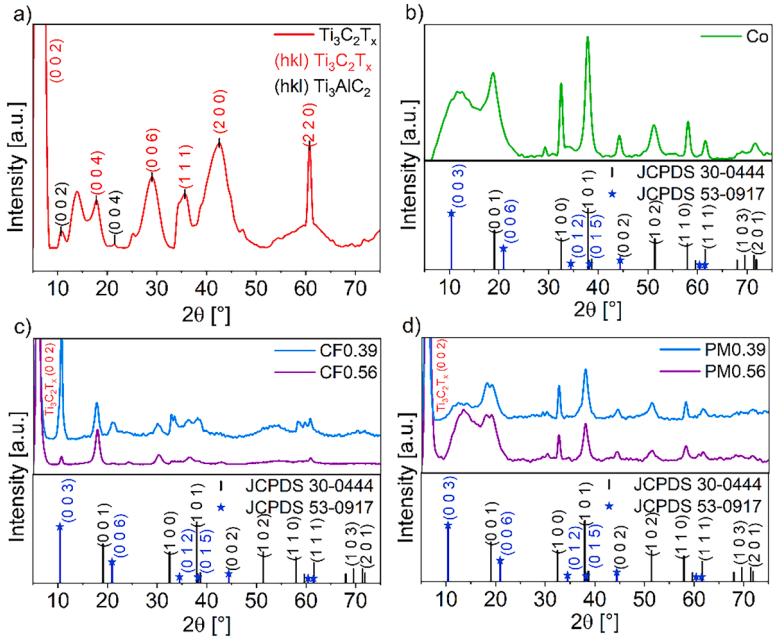

Fig. 3. X-ray diffractograms of a) $Ti_3C_2T_x$, b) pure Co, c) **CF0.39** and **CF0.56**, d) **PM0.39** and **PM0.56**. The JCPDS files no. 30–0443 and 53–0916 correspond to Co $(OH)_2$and hydrotalcite (Zincowoodwardite), respectively.

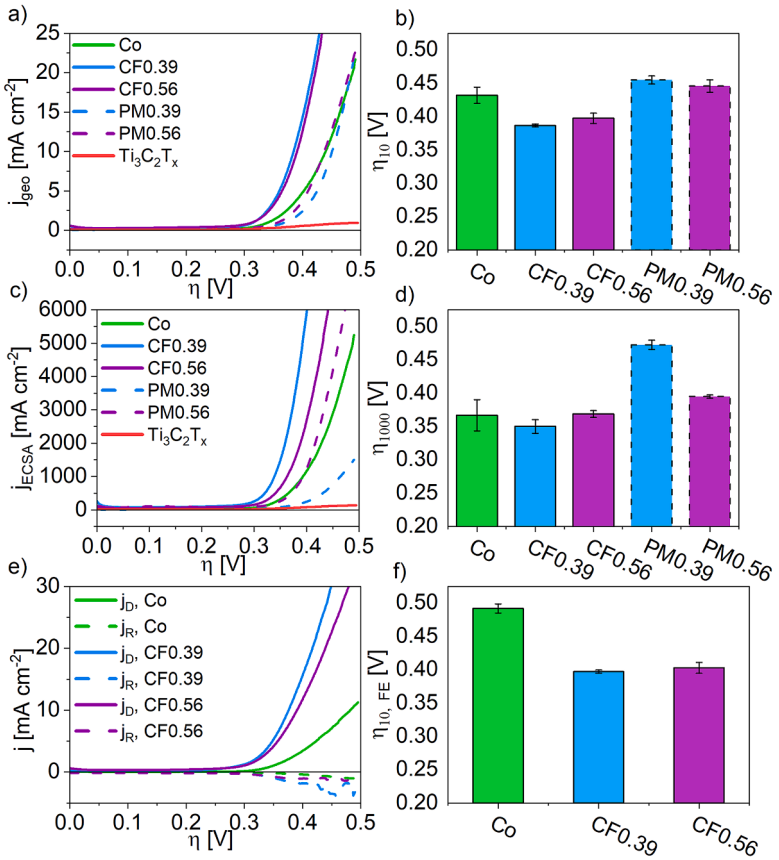

Fig. 5. Electrochemical evaluation of $Ti_3C_2T_x$, unsupported Co and physically mixed and chemically functionalized Co/$Ti_3C_2T_x$ composite materials, part 1. a) Linear sweep voltammograms (LSVs) (current normalized by the geometric area of the working electrode). b) Overpotential at 10 mA cm^{-2} (current normalized by the geometric area of the working electrode). c) LSVs normalized by the electrochemical surface area (ECSA). d) Overpotential at 1000 mA cm^{-2} (current normalized by ECSA). e) RRDE measurements for determining the Faradaic efficiency (FE). g) Overpotential at 10 mA cm^{-2} (current normalized by the geometric area of the working electrode and by FE).

NaOH is 0.04 mF/cm^2 [39]. To account for the much higher currents due to the ECSA typically being smaller than the geometric area, the current benchmark for the determination of the overpotential was set to 1 A. The LSV curves of the materials normalized by their ECSA and resulting overpotentials η_{1000} are depicted in Fig. 5c and d, which show the CF based materials are consistently better OER materials than the pure Co and PM materials. Interestingly, in Fig. 5c, at the higher range of the ECSA normalized current densities, the two CF materials and the PM0.56 all exhibit better OER performances than the pure Co and pure $Ti_3C_2T_x$.

Faradaic efficiency (FE) is a key parameter used to assess the selectivity of an electrocatalyst. In the case of the OER it provides a measure of how efficiently the electrochemical reaction converts electrical energy into oxygen gas while minimizing undesired side reactions. The rotating ring disk electrode (RRDE) coupled with a bi-potentiostat is a facile technique to determine FE [39]. In this method, oxygen gas that is produced at the disk is reduced at the ring which is held at a constant reducing potential. The resulting currents at both the disk and the ring are measured simultaneously and FE results from $-2i_R\ /(N{\cdot}i_D)$, where the factor 2 accounts for the 4/2 ratio of electrons transferred in the OER at the disk electrode and in the ORR at the ring electrode, i_R and i_D are the ring and disk currents at a potential of 0.35 V vs. Hg/HgO respectively, and N is the collection efficiency of the ring electrode [2]. The curves resulting from the RRDE experiments are depicted in Fig. 5e. It is evident that the composite materials **CF0.39** and **CF0.56** exhibit much higher FE than the pure Co sample (0.78 ± 0.08 and 0.81 ± 0.09 vs. 0.48 ± 0.18, respectively). Normalizing the current obtained from the RDE experiments with MXene supported Co materials under consideration of their respective FEs results in a remarkable reduction of the overpotential at 10 mA cm^{-2} by over 95 mV as presented in Fig. 5f. The overall relatively low FE values can be explained by the fact that oxygen bubbles evolving at the disk can accumulate in the catalyst layer before escaping into the bulk electrolyte thus reducing the measured ring current [40].

The correlation between the applied potential and the current change was examined by analysing the Tafel slopes of the materials (Fig. 6a). The unsupported Co sample exhibits a Tafel slope of 113 mV dec^{-1}. On the other hand, the chemically functionalized and physical mixed all exhibit Tafel slopes in the region of 80 – 66 mV dec^{-1}which is a significant decrease in Tafel slope to the pure Co with the addition of the $Ti_3C_2T_x$. Such a shift within the Tafel slope can be indicative of a change of the rate-determining step and in our case points to a factor limiting the OER towards potentials above 1.57 V vs. RHE. Conversely, no shift was observed in the Tafel slopes of the composite materials resulting in much shallower slopes at potentials above 1.57 V vs. RHE compared to unsupported Co sample (66 mV dec^{-1} and 77 mV dec^{-1} vs. 113 mV dec^{-1}). This improvement of the current response could be ascribed to the better conductivity of the catalyst layer, which is a known limiting factor in pure LDH materials [9].

The turnover frequency (TOF) is a good descriptor of the intrinsic activity of an OER electrocatalyst as it provides a metric of its ability to produce oxygen per active site per unit of time and can be calculated by $j_E/(4Q)$ where j_E is the current density measured at a potential associated with OER, Q is the voltametric charge density derived from the Co oxide anodic peak, as described in the experimental section, and the factor 4 is accounting for the number of electrons transferred per

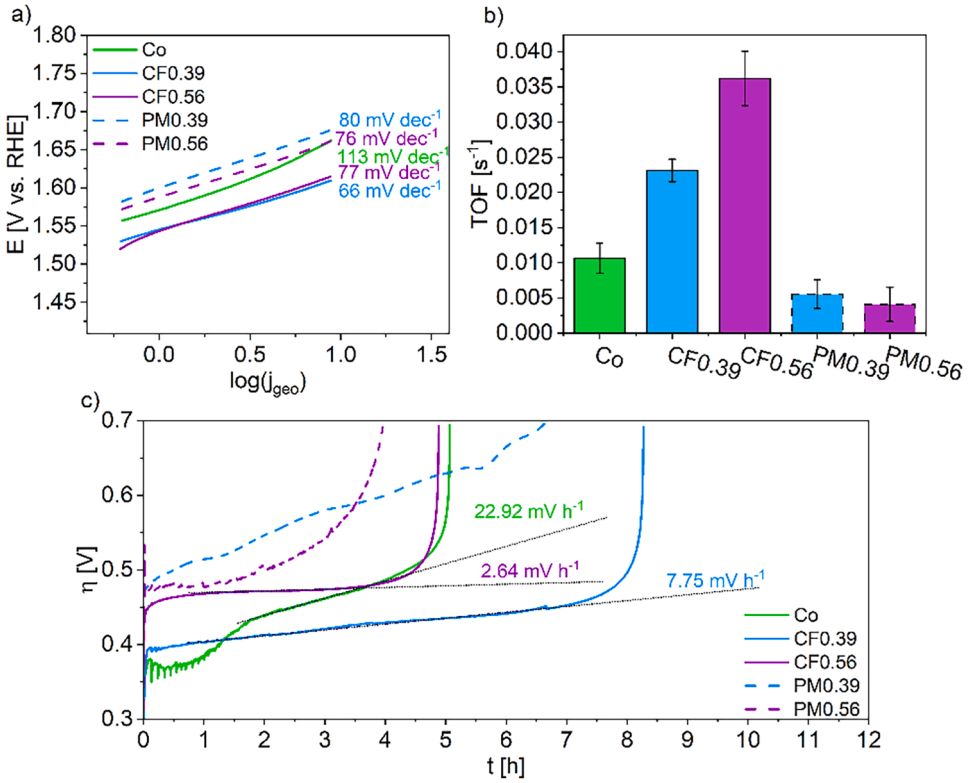

Fig. 6. Electrochemical evaluation of $Ti_3C_2T_x$, unsupported Co and physically mixed and chemically functionalized Co/$Ti_3C_2T_x$ composite materials, part 2. a) Tafel diagrams obtained from the LSV curves in Fig. 5a. b) Turnover frequencies (TOFs). c) Chronopotentiometry at 10 mA cm^{-1} over 12 h.

molecule of oxygen produced [41,42]. The TOFs of the pure Co sample and $Ti_3C_2T_x$ materials are presented in Fig. 6b. The TOF of pure Co (0.011 s^{-1}) is within the range of reported values for Co oxide materials [42,43]. The chemical functionalization with $Ti_3C_2T_x$ support causes a significant increase in TOF values compared to the unsupported Co, while the physically mixed composites show a slight decrease. Interestingly, **CF0.56** exhibits the best TOF of all materials. This stands in contrast to the current benchmark comparison where **CF0.39** showed slightly better OER performance, reinforcing the necessity to consider various metrics when evaluating the OER performance of materials.

Electrochemical Impedance Spectroscopy (EIS) was performed to estimate the effect of the $Ti_3C_2T_x$ on the charge transfer resistance (R_{ct}) (Figure S2). For OER catalysed by transition metal oxides, the diameter of the semi-circle formed by the Nyquist plot directly correlates with the charge transfer resistance of the catalyst [2]. The CF Co/MXene composites exhibit lower charge transfer resistances than the pure Co

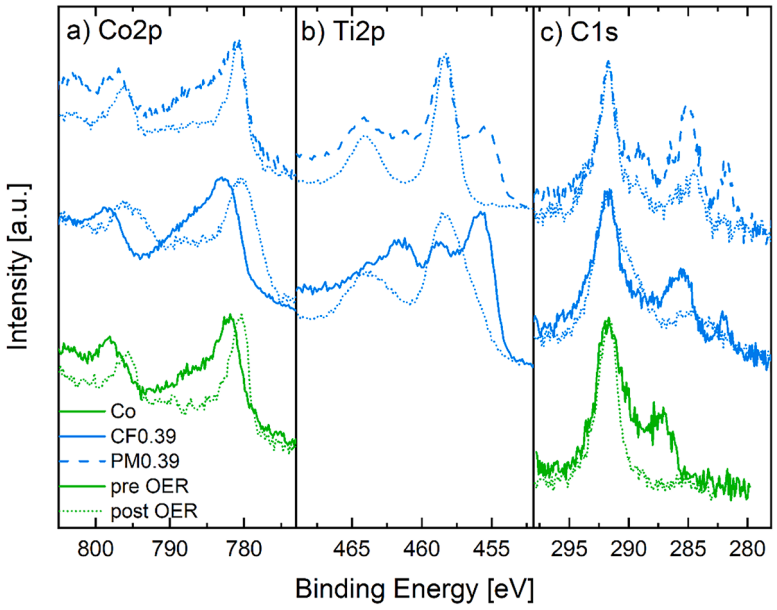

Fig. 7. X-ray Photoelectron spectra of pure Co and chemically functionalized (CF) composite materials before and after OER performance test. a) Co2p, b) Ti2p, and c) C1s core levels.

material during the OER which indicates a faster electron transfer during the OER when the Co and $Ti_3C_2T_x$ is chemically functionalized. Conversely, mere physical mixing of Co and MXene increased the charge transfer resistance with increasing MXene ratio thus pointing towards an inhibiting effect of the oxidised MXene i.e. TiO_2 (Ti(IV)) being formed as evident from the CV curves, Fig. 4. Finally, the stability of the composite and reference materials was probed by chronopotentiometry at a constant current density of 10 mA cm^{-2} until the material was degraded, Fig. 6c. The MXene-supported Co demonstrated a better over time performance, as evidenced by the slower increase of the overpotential of the samples **CF0.39** (7.75 mV h^{-1}) and **CF0.56** (2.64 mV h^{-1}) compared to the pure Co sample (22.92 mV h^{-1}).

The XPS spectra of the materials after OER performance tests are shown in Fig. 7 and Figure S3. In the Co2p spectra of both the pure Co sample and the composite materials (Fig. 7a) the satellite peak at 787–788 eV strongly decreases, which suggests a conversion of CoO or $Co(OH)_2$ into higher Co oxidation states, such as Co_3O_4, during the OER [31]. This oxidation is also consistent with the CV curves in Fig. 4. The reduction of the Ti-C signal in the Ti2p Fig. 7b) and C1s spectra (Fig. 7c) of the PM composite materials suggests the oxidation of $Ti_3C_2T_x$ under OER conditions. However, while the Ti-C signal is completely absent in the post OER spectra of the physically mixed samples it is still present in the chemically functionalized materials with reduced intensity. This shows that a noticeable degree of stabilization of the MXene was achieved by chemical functionalization with cobalt oxide/hydroxide which results in increased OER activity over the PM and pure Co materials.

4. Conclusion

In this study we successfully demonstrated that a significant enhancement in the oxygen evolution reaction (OER) performance of a Co oxide electrocatalyst is possible by incorporating $Ti_3C_2T_x$ MXene as a supporting material.

The observed reduction in overpotential by 40 mV at 10 mA cm^{-2} is a significant improvement of the electrocatalytic efficiency of the composite material. By scrutinizing key electrocatalytic parameters such as turnover frequency, stability, faradaic efficiency, and electrochemical surface area, we have demonstrated the capability of $Ti_3C_2T_x$ to improve the catalytic performance of Co oxide/hydroxide in metrics beyond the current benchmark. We experimentally determined Faradaic efficiencies of the materials and showed that factoring in the increased Faradaic efficiency, the MXene support led to a substantial reduction of the overpotential by 95 mV at 10 mA cm^{-2}. Furthermore, we calculated the turnover frequencies and found a trend of increasing catalytic activity towards higher MXene loadings, showing that not only the overpotential should be considered for optimizing the formulation of these composite materials. These results contribute to the growing understanding of MXene-supported transition metal oxides and pave the way for the rational design and optimization of future electrocatalytic materials driving the evolution of sustainable energy conversion technologies.

Declaration of competing interest

The authors declare that they have no known competing financial interests or personal relationships that could have appeared to influence the work reported in this paper.

Acknowledgements

The authors would like to thank R. Schwiddessen and M. Tovar from the Helmholtz Zentrum Berlin X-Ray Core Lab for providing access to their facility and training on the equipment. The authors would also like to thank K. Schwartzburg and M. Wollgarten from the Helmholtz Zentrum Berlin Microscopy core lab for providing access to their facility and training on the equipment.

Funding sources

We gratefully acknowledge the Helmholtz Association's Initiative and Networking Fund (Helmholtz Young Investigator Group VH—NG-1719) for the funding. Open Access funding enabled and organized by Projekt DEAL. M.P.B greatly acknowledges support from the German Federal Ministry of Education and Research in the framework of the project Catlab (03EW0015A/B). VN wishes to acknowledge funding from the European Research Council (CoG 3D2Dprint, GA 681544), Science Foundation Ireland (12/RC/2278_P2 and 16/RC/3872_P2, Frontiers for the Future 20/FFP-A/8950), and HORIZON-RIA 101091572 GREENCAP.

Supplementary materials

Supplementary material associated with this article can be found, in the online version, at doi:10.1016/j.electacta.2024.144269.

References

[1] E. Comission, A Hydrogen Strategy for A Climate Neutral Europe, 2020.
[2] M. Yu, E. Budiyanto, H. Tüysüz, Principles of water electrolysis and recent progress in cobalt-, nickel-, and iron-based oxides for the oxygen evolution reaction, Angew. Chem. Int. Ed. 61 (2022) e202103824.
[3] F. Dionigi, P. Strasser, NiFe-Based (Oxy)hydroxide catalysts for oxygen evolution reaction in non-acidic electrolytes, Adv. Energy Mater. 6 (2016) 1600621.
[4] S. Geiger, O. Kasian, B.R. Shrestha, A.M. Mingers, K.J.J. Mayrhofer, S. Cherevko, Activity and stability of electrochemically and thermally treated iridium for the oxygen evolution reaction, J. Electrochem. Soc. 163 (2016) F3132.
[5] J. Jiang, A. Zhang, L. Li, L. Ai, Nickel–cobalt layered double hydroxide nanosheets as high-performance electrocatalyst for oxygen evolution reaction, J. Power Sources 278 (2015) 445–451.
[6] F. Dionigi, Z. Zeng, I. Sinev, T. Merzdorf, S. Deshpande, M.B. Lopez, S. Kunze, I. Zegkinoglou, H. Sarodnik, D. Fan, A. Bergmann, J. Drnec, J.F.d. Araujo, M. Gliech, D. Teschner, J. Zhu, W.-X. Li, J. Greeley, B.R. Cuenya, P. Strasser, In-situ structure and catalytic mechanism of NiFe and CoFe layered double hydroxides during oxygen evolution, Nat. Commun. 11 (2020) 2522.
[7] L. Yan, Z. Du, X. Lai, J. Lan, X. Liu, J. Liao, Y. Feng, H. Li, Synergistically modulating the electronic structure of Cr-doped FeNi LDH nanoarrays by O-vacancy and coupling of MXene for enhanced oxygen evolution reaction, Int. J. Hydrogen Energy 48 (2023) 1892–1903.
[8] G. Fan, F. Li, D.G. Evans, X. Duan, Catalytic applications of layered double hydroxides: recent advances and perspectives, Chem. Soc. Rev. 43 (2014) 7040–7066.
[9] Y. Wang, D. Yan, S. El Hankari, Y. Zou, S. Wang, Recent progress on layered double hydroxides and their derivatives for electrocatalytic water splitting, Adv. Sci. 5 (2018) 1800064.
[10] F. Song, X. Hu, Exfoliation of layered double hydroxides for enhanced oxygen evolution catalysis, Nat. Commun. 5 (2014) 4477.
[11] M. Gong, Y. Li, H. Wang, Y. Liang, J.Z. Wu, J. Zhou, J. Wang, T. Regier, F. Wei, H. Dai, An advanced Ni–Fe layered double hydroxide electrocatalyst for water oxidation, J. Am. Chem. Soc. 135 (2013) 8452–8455.
[12] M. Görlin, J. Ferreira de Araújo, H. Schmies, D. Bernsmeier, S. Dresp, M. Gliech, Z. Jusys, P. Chernev, R. Kraehnert, H. Dau, P. Strasser, Tracking catalyst redox states and reaction dynamics in Ni–Fe oxyhydroxide oxygen evolution reaction electrocatalysts: the role of catalyst support and electrolyte pH, J. Am. Chem. Soc. 139 (2017) 2070–2082.
[13] M. Ghidiu, M.R. Lukatskaya, M.-Q. Zhao, Y. Gogotsi, M.W. Barsoum, Conductive two-dimensional titanium carbide 'clay' with high volumetric capacitance, Nature 516 (2014) 78–81.
[14] C. Zhang, B. Anasori, A. Seral-Ascaso, S.-H. Park, N. McEvoy, A. Shmeliov, G. S. Duesberg, J.N. Coleman, Y. Gogotsi, V. Nicolosi, Transparent, Flexible, and Conductive 2D Titanium Carbide (MXene) films with high volumetric capacitance, Adv. Mater. 29 (2017) 1702678.
[15] M. Benchakar, T. Bilyk, C. Garnero, L. Loupias, C. Morais, J. Pacaud, C. Canaff, P. Chartier, S. Morisset, N. Guignard, V. Mauchamp, S. Célérier, A. Habrioux, MXene supported cobalt layered double hydroxide nanocrystals: facile synthesis route for a synergistic oxygen evolution reaction electrocatalyst, Adv Mater Interfaces 6 (2019) 1901328.
[16] A.K.Sharma Navjyoti, V. Sharma, A.K. Debnath, V. Saxena, A. Mahajan, MXene supported nickel-cobalt layered double hydroxide as efficient bifunctional electrocatalyst for hydrogen and oxygen evolution reactions, J. Alloys Compd. 939 (2023) 168779.
[17] D. Vikraman, S. Hussain, L. Hailiang, K. Karuppasamy, P. Sivakumar, P. Santhoshkumar, J. Jung, H.-S. Kim, Spinel-structured metal oxide-embedded MXene nanocomposites for efficient water splitting reactions, Inorg Chem Front 9 (2022) 5903–5916.
[18] M. Naguib, M. Kurtoglu, V. Presser, J. Lu, J. Niu, M. Heon, L. Hultman, Y. Gogotsi, M.W. Barsoum, Two-dimensional nanocrystals produced by exfoliation of Ti_3AlC_2, Adv. Mater. 23 (2011) 4248–4253.

[19] X. Wang, C. Garnero, G. Rochard, D. Magne, S. Morisset, S. Hurand, P. Chartier, J. Rousseau, T. Cabioc'h, C. Coutanceau, V. Mauchamp, S. Célérier, A new etching environment (FeF3/HCl) for the synthesis of two-dimensional titanium carbide MXenes: a route towards selective reactivity vs. water, J. Mater. Chem. A 5 (2017) 22012–22023.
[20] M. Alhabeb, K. Maleski, B. Anasori, P. Lelyukh, L. Clark, S. Sin, Y. Gogotsi, Guidelines for synthesis and processing of two-dimensional titanium carbide (Ti3C2Tx MXene), Chem. Mater. 29 (2017) 7633–7644.
[21] J.L. Hart, K. Hantanasirisakul, A.C. Lang, B. Anasori, D. Pinto, Y. Pivak, J.T. van Omme, S.J. May, Y. Gogotsi, M.L. Taheri, Control of MXenes' electronic properties through termination and intercalation, Nat. Commun. 10 (2019) 522.
[22] Y. Lu, D. Fan, Z. Chen, W. Xiao, C. Cao, X. Yang, Anchoring Co3O4 nanoparticles on MXene for efficient electrocatalytic oxygen evolution, Science Bulletin 65 (2020) 460–466.
[23] M. Yu, S. Zhou, Z. Wang, J. Zhao, J. Qiu, Boosting electrocatalytic oxygen evolution by synergistically coupling layered double hydroxide with MXene, Nano Energy 44 (2018) 181–190.
[24] C. Hao, Y. Wu, Y. An, B. Cui, J. Lin, X. Li, D. Wang, M. Jiang, Z. Cheng, S. Hu, Interface-coupling of CoFe-LDH on MXene as high-performance oxygen evolution catalyst, Materials Today Energy 12 (2019) 453–462.
[25] H. Huang, B. Shen, M. Yan, H. He, L. Yang, Q. Jiang, G. Ying, Coupled spinel manganese−cobalt oxide and MXene electrocatalysts towards efficient hydrogen evolution reaction, Fuel 328 (2022) 125234.
[26] S. Ghorbanzadeh, S.A. Hosseini, M. Alishahi, CuCo2O4/Ti3C2Tx MXene hybrid electrocatalysts for oxygen evolution reaction of water splitting, J. Alloys Compd. 920 (2022) 165811.
[27] D. Tyndall, L. Gannon, L. Hughes, J. Carolan, S. Pinilla, S. Jaśkaniec, D. Spurling, O. Ronan, C. McGuinness, N. McEvoy, V. Nicolosi, M.P. Browne, Understanding the effect of MXene in a TMO/MXene hybrid catalyst for the oxygen evolution reaction, npj 2D Mater. Appl. 7 (2023) 15.
[28] ALS Japan, (2020).
[29] K. Li, M. Liang, H. Wang, X. Wang, Y. Huang, J. Coelho, S. Pinilla, Y. Zhang, F. Qi, V. Nicolosi, Y. Xu, 3D MXene architectures for efficient energy storage and conversion, Adv. Funct. Mater. 30 (2020) 2000842.
[30] M. Naguib, V.N. Mochalin, M.W. Barsoum, Y. Gogotsi, 25th anniversary article: mXenes: a new family of two-dimensional materials, Adv. Mater. 26 (2014) 992–1005.
[31] M.C. Biesinger, B.P. Payne, A.P. Grosvenor, L.W.M. Lau, A.R. Gerson, R.S.C. Smart, Resolving surface chemical states in XPS analysis of first row transition metals, oxides and hydroxides: cr, Mn, Fe, Co and Ni, Appl. Surf. Sci. 257 (2011) 2717–2730.
[32] M. Shekhirev, C.E. Shuck, A. Sarycheva, Y. Gogotsi, Characterization of MXenes at every step, from their precursors to single flakes and assembled films, Prog. Mater Sci. 120 (2021) 100757.
[33] A.C. Khot, T.D. Dongale, J.H. Park, A.V. Kesavan, T.G. Kim, Ti3C2-Based MXene oxide nanosheets for resistive memory and synaptic learning applications, ACS Appl. Mater. Interfaces 13 (2021) 5216–5227.
[34] R.G. Toro, M. Diab, T. de Caro, M. Al-Shemy, A. Adel, D. Caschera, Study of the effect of titanium dioxide hydrosol on the photocatalytic and mechanical properties of paper sheets, Materials (Basel) 13 (2020) 1326.
[35] P. Nayak, Q. Jiang, R. Mohanraman, D. Anjum, M.N. Hedhili, H.N. Alshareef, Inherent electrochemistry and charge transfer properties of few-layered two-dimensional Ti3C2Tx MXene, Nanoscale 10 (2018) 17030–17037.
[36] F. Švegl, B. Orel, M.G. Hutchins, K. Kalcher, Structural and spectroelectrochemical investigations of Sol-Gel derived electrochromic spinel Co3 O 4 Films, J. Electrochem. Soc. 143 (1996) 1532.
[37] E.B. Castro, C.A. Gervasi, Electrodeposited Ni–Co-oxide electrodes:characterization and kinetics of the oxygen evolution reaction, Int. J. Hydrogen Energy 25 (2000) 1163–1170.
[38] S. Anantharaj, S. Kundu, Do the evaluation parameters reflect intrinsic activity of electrocatalysts in electrochemical water splitting? ACS Energy Letters 4 (2019) 1260–1264.
[39] C.C.L. McCrory, S. Jung, J.C. Peters, T.F. Jaramillo, Benchmarking heterogeneous electrocatalysts for the oxygen evolution reaction, J. Am. Chem. Soc. 135 (2013) 16977–16987.
[40] I.S. Filimonenkov, S.Y. Istomin, E.V. Antipov, G.A. Tsirlina, E.R. Savinova, Rotating ring-disk electrode as a quantitative tool for the investigation of the oxygen evolution reaction, Electrochim. Acta 286 (2018) 304–312.
[41] B.S. Yeo, A.T. Bell, Enhanced activity of gold-supported cobalt oxide for the electrochemical evolution of oxygen, J. Am. Chem. Soc. 133 (2011) 5587–5593.
[42] R.L. Doyle, I.J. Godwin, M.P. Brandon, M.E.G. Lyons, Redox and electrochemical water splitting catalytic properties of hydrated metal oxide modified electrodes, Phys. Chem. Chem. Phys. 15 (2013) 13737–13783.
[43] X. Deng, H. Tüysüz, Cobalt-oxide-based materials as water oxidation catalyst: recent progress and challenges, ACS Catal 4 (2014) 3701–3714.